Experimental Analysis of Partial Evaporation Micro-ORC for low-temperature Heat Recovery

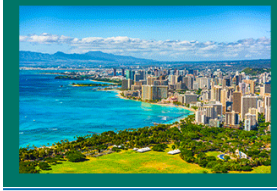

Journal of Physics: Conference Series **2511** (2023) 012015 doi:10.1088/1742-6596/2511/1/012015

Experimental Analysis of Partial Evaporation Micro-ORC for low-temperature Heat Recovery

S Ottaviano, C Poletto, A De Pascale and M Bianchi

Department of Industrial Engineering (DIN) – University of Bologna,
Viale del Risorgimento 2, 40136 Bologna, Italy

saverio.ottaviano2@unibo.it

Abstract. In this paper, we present an experimental assessment of the performance of a partial evaporating organic Rankine cycle (PE-ORC) power system. The system converts low temperature heat into electrical energy, with a power size around 1 kW, thus suitable for micro-generation in the residential sector. Although the test bench was designed for operating with superheated vapour at the expander inlet, it has demonstrated to be able to work with the expansion occurring entirely in two-phase condition. Since the direct measurement of the vapour quality is not possible using the sensors installed in the test rig, the state of the fluid in the two-phase condition is estimated by means of the thermal balance at the heat exchangers, so the thermodynamic cycle can be evaluated. Temperatures of the heat source in the range between 40 °C and 75 °C have been tested, and for each temperature value the vapour quality at the expander inlet has been varied by regulating the feed-pump rotating speed. Experimental data are provided regarding the performance of the overall cycle, of the heat exchangers, of the expander and of the feed-pump. It was observed that the effectiveness of the evaporator and the efficiency of the pump are improved with respect to the operation with superheated vapour at the expander inlet. However, the overall performance is lower, especially due to the high ratio of the pump consumption over the expander produced power, commonly called back work ratio (BWR). The latter, under some boundary conditions, has resulted higher than the unit, meaning that the system is not able to produce net electrical power. The aim of the paper is to identify the design characteristics required by a micro-ORC energy system in order to enhance its performance in the PE operating mode.

Nomenclature

Symbols and acronyms

BWR	Back Work Ratio [-]	p	Pressure [bar]
c	Specific heat [kJ/kg K]	PE	Partial evaporation
DE	Dry expansion	$\dot{Q}$	Thermal power [kW]
η	Efficiency [%]	RV	Read value
ε	Heat transfer effectiveness [-]	ρ	Density [kg/m3]
f	Frequency [Hz]	T	Temperature [°C]
FS	Full Scale	τ	Temperature difference [K]
h	Specific enthalpy [kJ/kg]	U	Uncertainty
$\dot{m}$	Mass flow rate [kg/s]	$\dot{V}$	Volume flow rate [l/s]
N	Rotational speed [rpm]	$\dot{W}$	Power [W]
ORC	Organic Rankine Cycle	x	Vapor quality in the two-phase mixture

Subscripts		L	Liquid phase (saturation)
CW	Cold water	net	Net
cond	Condensation/condenser	out	Outlet
el	Electric	p, pump	Pump
eco	Economizer	rec	Recuperator
eva	Evaporator	sc	Sub-cooling
exp	Expander	sh	Superheating
HW	Hot water	V	Vapor phase (saturation)
in	Inlet	vap	Vaporization / vaporizer

1. Introduction

Organic Rankine cycle is considered the most suitable technology for the exploitation of low-temperature heat sources. The ORC with partial evaporation and two-phase expansion is gaining attention due to some distinctive characteristics that make it profitable for the exploitation of low-grade heat sources. If the expansion occurs entirely in wet conditions, generally two configurations are possible: the trilateral flash cycle (TFC), in which the fluid enters the expander in the state of saturated liquid, and the partially evaporated organic Rankine cycle (PE-ORC), in which the vaporization of the working fluid is interrupted at a certain value of the vapour quality.

The interest in studying ORC systems with trilateral cycle or partial evaporation regards the possibility to achieve higher conversion efficiency from heat sources with a finite capacity [1] [2]. Indeed, eliminating or reducing the isothermal heat of vaporization allows for an improvement of the temperature match between the heat source and the working fluid, resulting in higher usage of the energy available from the heat source. This condition reduces heat transfer losses and increases the heat exchanger effectiveness. It was observed that the largest convenience is achieved with low-temperature heat sources [3].

On the contrary, the performance of the expander in wet conditions may be lower than in the case of dry expansion, resulting in lower power output at a given mass flow rate of the working fluid. Moreover, the expansion occurring in the two-phase condition, in general, may lead to erosion of the expander materials that reduces the machine lifetime [4]. With respect to turbines, volumetric expanders (such as the machine used for this study) can withstand better the expansion occurring, partially or completely, in the two-phase condition [5].

When dealing with partial evaporation, a critical issue is related to the determination of the thermodynamic properties of the working fluid at each section of the circuit. Indeed, differently from the dry expansion (DE) case, in which the working fluid is in single-phase state in all the measuring sections of the circuit, and the properties are calculated directly from temperature and pressure measured values, in the partially evaporated cycle the fluid is in two-phase conditions in at least two sections (inlet and outlet of the expander), three in case a recuperator is present. In such points, the knowledge of temperature and pressure is not sufficient to determine the corresponding fluid enthalpy or its vapour quality.

To the Authors' knowledge, technologies allowing to directly measure the vapour quality of saturated fluid are not common in the market. The company Cooltech Finland Oy, in the field of industrial refrigeration machinery, proposes a vapour quality sensor to optimize processes in refrigeration systems [6]; however, this product allows to detect a vapour quality limited in the range between 0.80 and 1.00, and with temperatures lower than 50 °C, which are quite limiting for the current experimental investigation.

Therefore, to estimate the complete thermodynamic states of the system working with partial evaporation, it is necessary to apply an indirect calculation through energy balances. Dawo et al, in the experimental comparison between the ORC and the PE-ORC operating modes [7], compute the organic fluid enthalpy at the outlet of the evaporator applying the thermal balance on the hot water side (which serves as heat source), then they obtain the vapour quality through REFPROP library. In a similar way, Iqbal et al., in their experimental study involving a trilateral flash cycle [8], use the thermal balance on the high-pressure heat exchanger to determine the thermodynamic state of the

organic fluid at the beginning of the expansion process. Noël et al. propose two similar methods to evaluate the effective vapour quality of the working fluid at the compressor suction port in residential heat pumps: since the assumption of saturated vapour at the compressor inlet leads to highly overestimate the working fluid mass flow rate, the Authors compute the vapour quality and the effective mass flow rate through two iterative methods involving both the energy balance on the compressor, and the volumetric efficiency or the global efficiency respectively [9].

The aim of this study is to present the results of an experimental campaign performed on a kW-size ORC in PE conditions. The investigation is conducted for three levels of the heat source temperature (45-60-75 °C), with special attention to the assessment of the vapour quality at the expander inlet, and to the effects of its variation on the cycle performance. The experimental data presented here are a subset of those recently reported in [10], in which a more comprehensive experimental analysis was included, aimed at providing an extensive characterization of the ORC in PE working mode, evaluating real issues at operation and control level.

2. System description

The layout and specifics of the test rig are reported in Figure 1 and in Table 1 [11]. The ORC system is based on a recuperative configuration and operates with HFC-134a as working fluid with a total charge of 22 kg. The main components of the ORC circuit are a reciprocating pistons expander, an external gear pump, two brazed plate heat exchangers (the evaporator and the recuperator), a shell and tube condenser and a liquid receiver. The hot source is composed of an electric water heater with nominal thermal power of 42 kW, consisting of a 500-litres tank provided with five heating elements, which can be activated separately to regulate the available thermal input. The pressure inside the hot water circuit is maintained above the ambient pressure (between 1 and 2 bar), in order to avoid local vaporization phenomena at high temperatures, which may cause the cavitation of the centrifugal pump P2. The water temperature at the evaporator inlet can be regulated using the automatic three-way valve (AV1) placed at the heater outlet, which mixes the hot water with colder water coming from the evaporator. The water flow rate is adjusted by acting on the motorized ball valve (AV2).

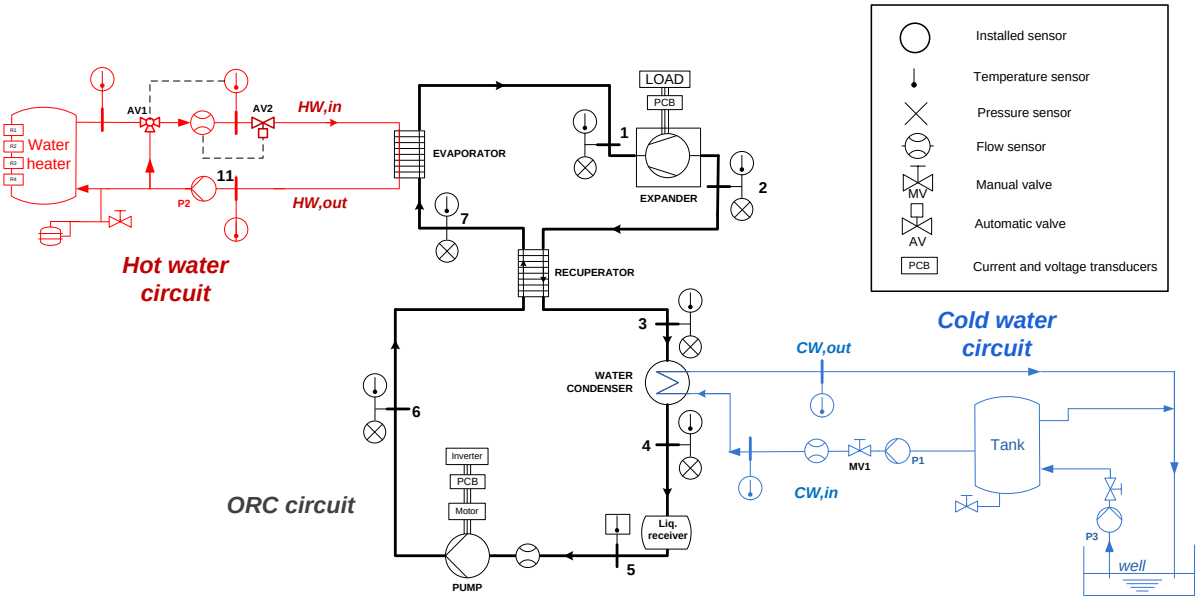

Figure 1. Layout of the micro-ORC test bench

Table 1. Main specifics of the micro-ORC components

COMPONENT	MODEL	FEATURES
EVAPORATOR	ONDA S202	Plate heat exchanger with 64 plates
RECUPERATOR	ONDA S202	Plate heat exchanger with 19 plates
CONDENSER	ONDA CT292-1100	Shell-and-tube heat exchanger with 4 passages
EXPANDER	Radial piston prototype (STARENGINE) [13]	Three radial cylinders at 120°, displacement = 230 cm^3, direct coupling with generator
PUMP	External gear prototype (STARENGINE)	Displacement = 50 cm^3, driven by three-phase 1.5 kW asynchronous motor with inverter. Variable speed between 90 rpm and 300 rpm
GENERATOR	Magnetic NGB 145 M-SA	Three-phase permanent magnet synchronous generator, 380 V, 5.2 A, 8 poles
LOAD	Pure resistive	Five parallel loads, each made of three light bulbs, connected in *delta* with the generator

The list and specifications of the measurement devices are collected in Table 2. In short, the list of measured variables includes temperatures, pressures and mass flow rate in ORC circuit, temperatures and volume flow rates in hot and cold water circuits, electric current and voltage of expander and feed-pump for power and frequency assessment. The number and positions of the sensors are detailed in Figure 1 and in Table 2. All pressure transducers and thermocouples are calibrated periodically at the laboratory, together with the complete measurement chain (cables and acquisition devices), in order to decrease the uncertainty related to the performance assessment. The acquisition system is developed on a National Instruments CompactRIO in LabVIEW environment. The properties of the organic fluid are computed thanks to the open-source library CoolProp [12], which is integrated into the acquisition software.

Table 2. Sensor specifics

PHYSICAL QUANTITY	LAYOUT POINT (FIGURE 1)	SENSOR	CALIBRATION RANGE	COTS ACCURACY*	OUTPUT SIGNAL AND MODULE
ORC TEMPERATURES	1, 2, 3, 4, 6, 7	T-type thermocouple, 1 mm probe	0–90 °C	±0.5 °C	±80 mV - NI9213 (Thermocouple input)
HOT WATER TEMPERATURES	HW_{in}, HW_{out}, HW_{boil}	K-type thermocouple, 1 mm probe	0–90 °C	±0.5 °C	
COLD WATER TEMPERATURES	CW_{in}, CW_{out}				
ORC PRESSURES	1, 6, 7	Pressure transducer, Honeywell FP2000	0–30 bar	±0.25% FS	0–5 V - NI9201
	2, 3, 4, 5		0–10 bar		
ORC MASS FLOW RATE	5	Coriolis mass flow meter, E+H Promass	0.05–1.00 kg/s	±0.3% RV	4–20 mA - NI9203
ORC DENSITY			10–1300 kg/m3	±0.1 kg/m3	
HOT WATER FLOW RATE	HW_{in},	Magnetic flow meter, E+H Promag	0–6.4 l/s	±0.5% RV	
COLD WATER FLOW RATE	CW_{in}		0–9.8 l/s		
ELECTRIC VOLTAGE AND CURRENT	Expander generator and pump motor supply lines	PCB-mounted Hall effect voltage and current transducers	0–400 V	±0.1% RV	0–4 V - NI9215
			0–5A	±0.2% RV	

*Component Off-the-Shelf (COTS) accuracy: it refers to the instrument accuracy, as indicated on the datasheet, before individual calibration or calibration of the measurement chain.

3. Methodology

3.1. Assessment of the organic fluid thermodynamic states in PE working mode

The thermodynamic state of the working fluid at the sections of the circuit in which the fluid is in a single-phase (subcooled liquid) zone is determined through CoolProp library, with temperature and pressure values as inputs. This is expressed by Equation (1), where the term *CPfun* indicates the CoolProp function, and the subscript *i* recall the number of the ORC section, according to the layout in Figure 1.

$$h_i = CPfun(p_i, T_i) \qquad i = 4, 5, 6, 7 \tag{1}$$

On the contrary, in the sections where the organic fluid is in two-phase conditions, it is not possible to directly obtain its thermodynamic properties, through the CoolProp function, from the measurements of temperature and pressure. Therefore, the specific enthalpy of the working fluid at the evaporator outlet (expander inlet, h_1) is computed applying the thermal balance at the evaporator (Eq. (2)):

$$h_1 = h_7 + \frac{\dot{V}_{HW} \cdot \rho_{HW}}{\dot{m}_{wf}} \cdot c_{HW} \cdot \left(T_{HW,in} - T_{HW,out}\right) \tag{2}$$

In Eq. (2), the symbols $\dot{V}_{HW}$, ρ_{HW} and c_{HW} represent, respectively, the volume flow rate, the density and the specific heat of the hot water, and they are computed via CoolProp as functions of water temperature and pressure. The enthalpy of the fluid entering the evaporator (h_7) is obtained directly with CoolProp, as function of measured temperature and pressure (T_7 and p_7, respectively), since the fluid is in the subcooled liquid zone at the evaporator inlet (Eq. (1)).

In similar way as for h_1, the fluid enthalpy at the condenser inlet (h_3) is calculated by means of the energy balance at the condenser (Eq. (3), with the symbols $\dot{V}_{CW}$, ρ_{CW} and c_{CW} corresponding to the volume flow rate, the density and the specific heat of cold water, respectively). The enthalpy of the subcooled liquid at the condenser outlet (h_4) is determined by means of the CoolProp library as function of temperature and pressure (T_4 and p_4, respectively). Eventually, the enthalpy value at the expander outlet (h_2) is obtained from Equation (4), representing the thermal balance at the recuperator, assuming constant mass flow rate of the working fluid in the whole ORC circuit.

$$h_3 = h_4 + \frac{\dot{V}_{CW} \cdot \rho_{CW}}{\dot{m}_{wf}} \cdot c_{CW} \cdot \left(T_{CW,out} - T_{CW,in}\right) \tag{3}$$

$$h_2 = h_3 + (h_7 - h_6) \tag{4}$$

With the same approach, the enthalpies values of the organic fluid in the high-pressure side (points 6 and 7) are directly determined via CoolProp, as function of measured temperatures and pressures.

Once the enthalpy has been computed in all the sections of the circuit, the thermodynamic cycle of the PE-ORC is fully determined. The values of the vapour quality in the two-phase points (1, 2 and 3) are obtained using pressure and enthalpy as inputs to the CoolProp function, as indicated by Equation (5).

$$x_i = CPfun(p_i, h_i) \qquad i = 1,2,3 \tag{5}$$

In order to verify the accuracy of the energy balance to determine the thermodynamic states of the organic fluid in the two-phase sections, the same methodology has been applied to the experimental data obtained in dry expansion (DE) working mode. The specific enthalpies in sections 1, 2 and 3 of the cycle have been calculated through the thermal balance at the heat exchangers (according to Eq.s (2), (3) and (4)), and compared with the values provided by CoolProp library, as functions of measured temperatures and pressures. Figure 2 and Figure 3 confirm that the accuracy reached with the energy balance method is acceptable for the purpose of this study. The parity plot of the specific

enthalpy at the expander inlet in DE mode, in Figure 2, highlights that the error made with the energy balance calculation is always lower than 5 % with reference to the direct evaluation via CoolProp. Moreover, Figure 3 shows that the more accurate value computed via CoolProp lies within the uncertainty range of the calculated value through the thermal balance.

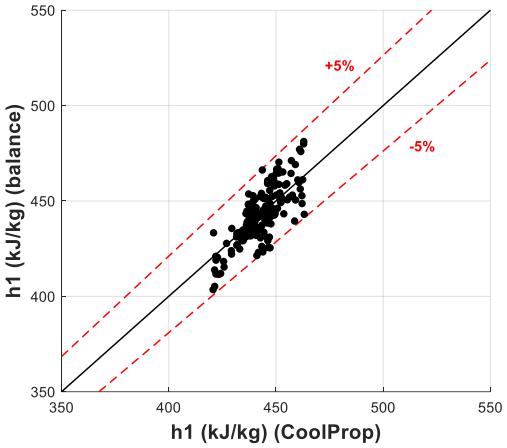

Figure 2. Parity plot of the specific enthalpy at the expander inlet (h_1) in DE mode: h_1 computed through the thermal balance of the evaporator versus h_1 from CoolProp.

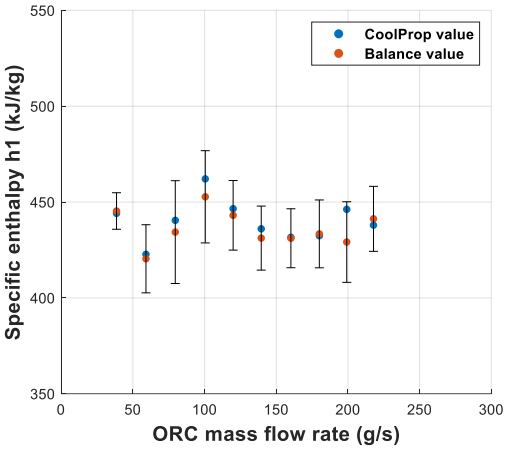

Figure 3. Specific enthalpy at the expander inlet (h_1) in DE mode versus working fluid mass flow rate.

3.2. Uncertainty quantification

The assessment of the working fluid thermodynamic state at each section of the cycle is affected by a certain level of uncertainty due to the sensor/probe characteristics, installation, calibration procedures. Furthermore, in the two-phase region the fluid thermodynamic properties are also affected by the propagation of the uncertainties of multiple measurements, due to the calculation process based on thermal balances and CoolProp library. Each variable and calculation, involved in the process, adds a contribution to the total uncertainty of the calculated state properties.

The uncertainty calculation of the ORC performance parameters, which has been described in [14], is based on the procedure reported in the standard ISO/IEC Guide 98 and EA-4/02M. The propagation of the uncertainty is realized by means of the classic procedure based on the propagation rule: this rule allows to calculate the uncertainty of a variable by considering the uncertainties of all the variables from which it depends. For instance, if y is a variable computed as a function of x and z, the uncertainty of y, δy, is evaluated through Equation (6).

$$\delta y = \sqrt{\left(\frac{\partial y}{\partial x}\right)^2 \delta x^2 + \left(\frac{\partial y}{\partial z}\right)^2 \delta z^2} \tag{6}$$

where δx and δz are the uncertainties of x and z, while $\frac{\partial y}{\partial x}$ and $\frac{\partial y}{\partial z}$ are the partial derivatives of y with reference to respectively x and z.

According to [14], three standards for the computation of the uncertainty contributions can be distinguish on the basis of the level of accuracy: the basic approach is characterized by the off-the-shelf accuracy of the sensor, probes and acquisition module.

The off-the-shelf uncertainty analysis approach is the simplest one as no calibration process is required, but the uncertainty assessment is based on the data reported in each data sheet of probes/sensors and acquisition modules.

In the field-calibrated uncertainty approach, pressure sensors and temperature probes are calibrated on-field by means of a standard procedure, using a pressure calibrator and thermostatic furnace, respectively, which are in turn calibrated towards a primary laboratory standard certified in agreement

with the Italian Accreditation Body (Accredia). In this case, two uncertainty contributions are considered, one is the reference uncertainty of the certified laboratory standard (type B), the other is related to the standard deviation of the set of data (type A). This type of calibration is not able to eliminate signal noise and to control the environmental conditions.

The third approach is the lab-scale uncertainty analysis, in which pressure sensors and temperature probes are calibrated by means of a standard procedure in a controlled (lab-scale) condition.

The uncertainty contribution to measurement chain of temperature and pressure is different in the three approaches: for instance, in the first approach the main contribution to the uncertainty is provided by the measurement performance of the acquisition module. In the on-field approach, the uncertainty is mostly affected by sensor/probe performance, because of the effects of uncontrolled environment conditions. Eventually, in the lab-scale approach a relevant contribution to the uncertainty chain is provided by the accuracy of the calibrator (Figure 4).

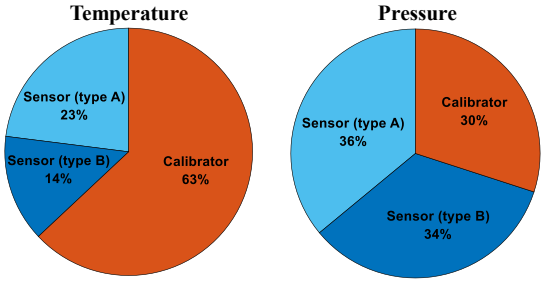

Figure 4. Uncertainty contributions of temperature and pressure measurement chain

Amongst these three standards, the present case belongs to the third approach, in which the measurement uncertainty is represented by the reference uncertainty of the certified laboratory. Temperature and pressure sensors are calibrated periodically at the UNIBO laboratory, in their operating ranges, with certified instruments (MicroCal PM200+). The uncertainty contributions for the flow meters, instead, are provided by the manufacturer, hence the method of uncertainty assessment is the off-the-shelf.

Once the uncertainties of pressure and temperature have been estimated, the uncertainty of the specific enthalpy can be computed according to the general rule of uncertainty propagation (Eq. (6)), which is modified in the Equation (7):

$$\delta h = \sqrt{\left(\frac{\partial h}{\partial p}\right)^2 \delta p^2 + \left(\frac{\partial h}{\partial T}\right)^2 \delta T^2} \tag{7}$$

where the partial derivatives of enthalpy, with reference to pressure and temperature (independent variables), are estimated using the CoolProp library.

The uncertainty of the enthalpy at the outlet of the evaporator (h_1) results from the propagation of the uncertainties of the enthalpy at the inlet (h_7), the organic fluid mass flow rate ($\dot{m}_{wf}$) and the evaporator exchanged thermal power ($\dot{Q}_{eva}$):

$$\delta h_1 = \sqrt{\left(\frac{\partial h_1}{\partial h_7}\right)^2 {\delta h_7}^2 + \left(\frac{\partial h_1}{\partial \dot{Q}_{eva}}\right)^2 {\delta \dot{Q}_{eva}}^2 \left(\frac{\partial h_1}{\partial \dot{m}_{wf}}\right)^2 {\delta \dot{m}_{wf}}^2} \tag{8}$$

The uncertainty of the thermal power exchanged at the evaporator ($\dot{Q}_{eva}$) is computed as follows (Eq. (9)):

$$\delta \dot{Q}_{eva} = \sqrt{\left(\frac{\partial \dot{Q}_{eva}}{\partial \dot{V}_{HW}}\right)^2 {\delta \dot{V}_{HW}}^2 + \left(\frac{\partial \dot{Q}_{eva}}{\partial h_{HW,in}}\right)^2 {\delta h_{HW,in}}^2 + \left(\frac{\partial \dot{Q}_{eva}}{\partial h_{HW,out}}\right)^2 {\delta h_{HW,out}}^2} \tag{9}$$

The same method is adopted to calculate the uncertainty for all the performance indexes.

4. Results and Discussion

The experimental points shown in the next figures have been obtained with three levels of heat source temperature ($T_{HW,in}$), namely 45 °C, 60 °C and 75 °C. Maintaining constant $T_{HW,in}$, the feed-pump rotational speed was regulated to vary the mass flow rate of the working fluid ($\dot{m}_{wf}$). The value of $\dot{m}_{wf}$ increases linearly with the pump speed, as shown in Figure 5, which reveals also that a smaller effect on the flow rate is given by the heat source temperature at constant speed.

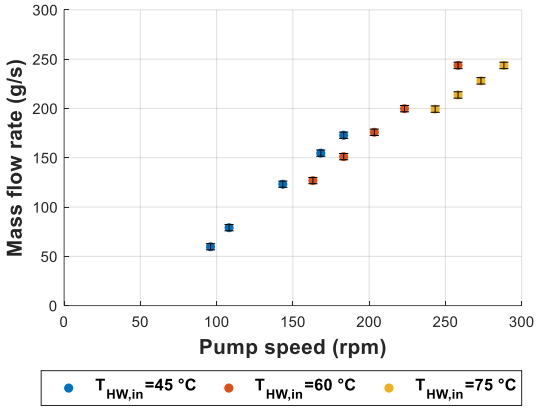

Figure 5. Working fluid mass flow rate ($\dot{m}_{wf}$) versus pump speed, at different heat source temperatures ($T_{HW,in}$).

Differently from the condition of dry expansion, in the operation with partial evaporation the increment of the mass flow rate at constant $T_{HW,in}$ produces only a little variation of the evaporation pressure (p_1), which depends mainly on the temperature of the heat source (Figure 6). A secondary effect on p_1 is given by the flow rate of the hot water, as explained in Figure 8a. The average value of the pressure p_1 results close to 11 bar, 16 bar and 21 bar, for the heat source temperature equal, respectively, to 45 °C, 60 °C and 75 °C.

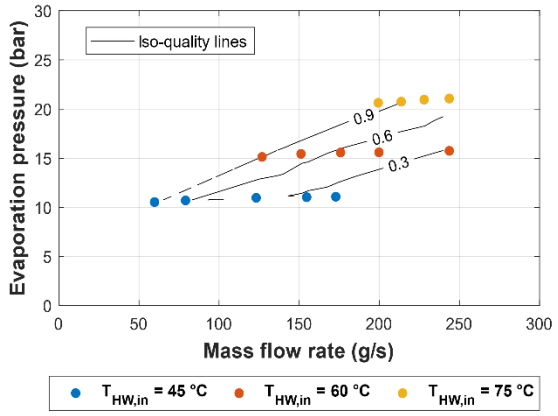

Figure 6. Evaporation pressure (p_1) versus working fluid mass flow rate ($\dot{m}_{wf}$), at different heat source temperatures ($T_{HW,in}$).

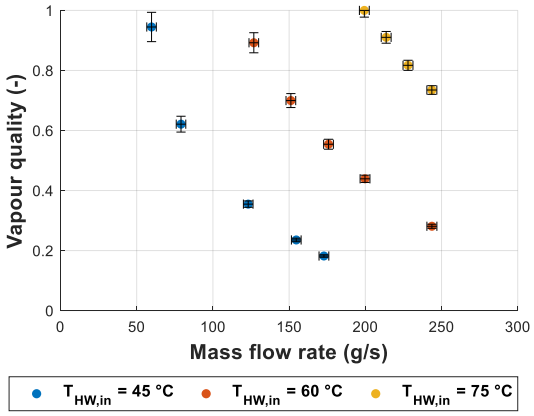

Figure 7. Vapour quality at the expander inlet (x_1) versus working fluid mass flow rate ($\dot{m}_{wf}$), at different heat source temperatures ($T_{HW,in}$).

As shown in Figure 7, the main effect of the increment of $\dot{m}_{wf}$ is the reduction of the vapour quality of the working fluid at the expander inlet (x_1), while the pressure at the same circuit section

(i.e. the evaporation pressure, p_1) remains almost constant. The minimum quality is close to 0.2, obtained with heat source temperature equal to 45 °C.

The effect of the variation of the hot water flow rate and of the organic fluid flow rate is explained in the evaporator heat transfer diagrams in Figure 8. In Figure 8a, the two represented working conditions are characterized by the same value of heat source temperature ($T_{HW,in} \cong 45\ °C$), and constant pump rotational speed around 110 rpm (hence, in first approximation, also the mass flow rate of the organic fluid is constant, around 80 g/s). The value of the hot water flow rate ($\dot{V}_{HW}$) is changed from 0.64 l/s (continuous line) to 2.5 l/s (dashed line), causing an increment of the evaporation temperature of almost 2 K, which corresponds to a rise of the evaporation pressure of about 0.5 bar, from 10.5 bar to 11.0 bar. The increment of p_1 is related to the slope of the water curve in the diagram, which is reduced by increasing the water flow rate, with the pinch point temperature difference kept at $\cong 1\ K$). The transferred thermal power increases from 9.7 kW to 11.3 kW, as shown in Figure 8a. Since the position of the pinch point in the diagram does not change, the increment of the thermal power is associated with the increment of the power exchanged in the vaporization zone, while the economizer heat remains the same. This means that the two conditions lead to different values of the vapour quality at the evaporator outlet, which is reduced as the water flow rate decreases. In the case shown in Figure 8a, the value of the quality x_1 changes from 0.6 to 0.75.

Figure 8b presents a different case of transition, in which the temperature and the flow rate of the hot water are maintained constant, equal to 45 °C and to 1.0 l/s respectively. The speed of the feed-pump is instead regulated from 96 rpm to 183 rpm (continuous and dashed lines respectively), affecting the organic fluid mass flow rate that increases from 60 g/s to 170 g/s. The effect of the increment of $\dot{m}_{wf}$ is the variation of the evaporation temperature of almost 2 K, corresponding to a rise of the pressure from 10.5 bar to 11.1 bar. Differently from the case of Figure 8a, the increment of the evaporation pressure is related to the reduction of the pinch point temperature difference, which decreases from 1.3 K to 0.5 K, as the mass flow rate increases. The position of the pinch point in the diagram shifts to the right, leading to a reduction of the heat transferred in the vaporizer zone, in favour of the economizer exchanged thermal power. Hence, the value of the quality x_1 is decreased by increasing the mass flow rate (from 0.94 to 0.2 in the case shown in Figure 8b).

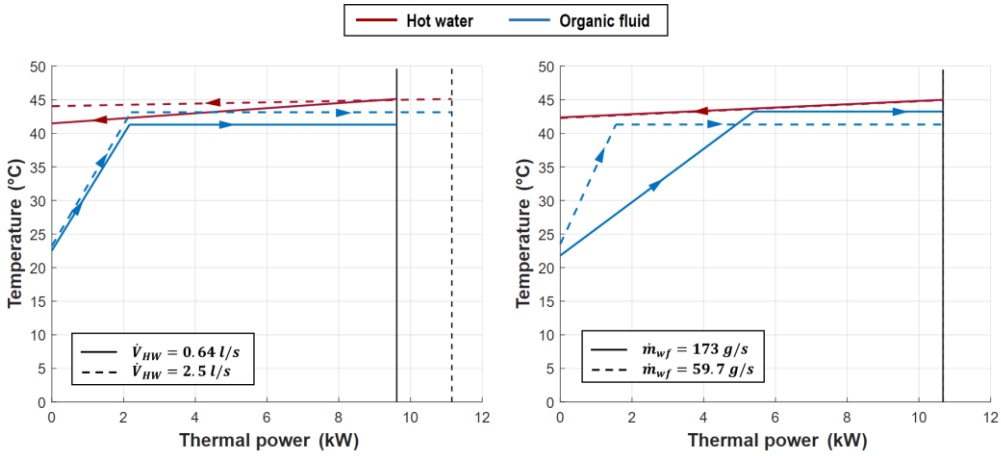

Figure 8. Effect of the variation of the hot water flow rate (left) and of the working fluid flow rate (right) in the heat transfer diagram, at constant heat source temperature of 45 °C.

The trend of the condensation pressure (p_2) is presented in Figure 9 as function of $\dot{m}_{wf}$ and $T_{HW,in}$. The value of p_2 shows a quasi-constant trend at constant heat source temperature, especially at $T_{HW,in}$ equal to 45 °C and 60 °C, while at 75 °C a very slight increment can be observed with the mass flow

rate. The average value of p_2 is around 6.2 bar. 7.2 bar and 8 bar, for the heat source equal to 45 °C, 60 °C and 75 °C respectively.

The thermal power transferred in the evaporator ($\dot{Q}_{eva}$), shown in Figure 10, reveals a considerably different trend with respect to the operation in DE mode, in which $\dot{Q}_{eva}$ depended almost linearly on the mass flow rate [11]. In PE mode, the value of $\dot{Q}_{eva}$ depends mainly on the heat source temperature, while the effect of the mass flow rate is minimal.

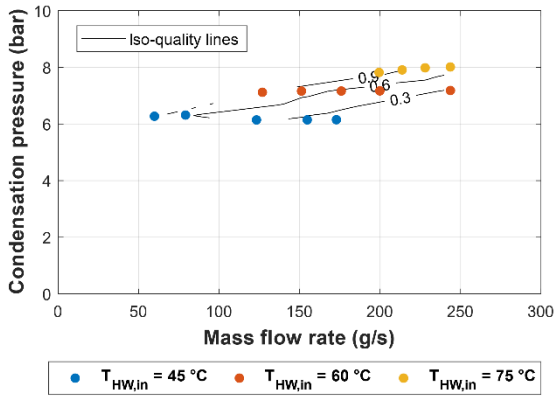

Figure 9. Condensation pressure (p_2) versus working fluid mass flow rate ($\dot{m}_{wf}$), at different heat source temperatures ($T_{HW,in}$).

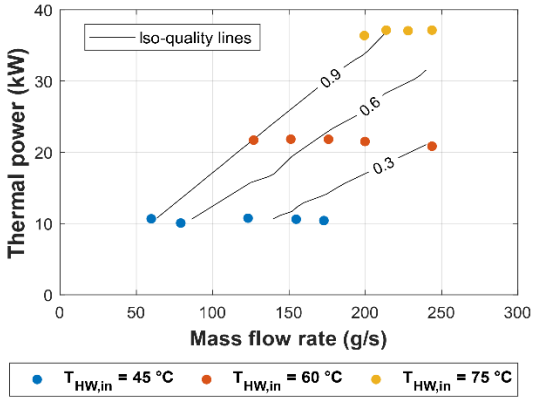

Figure 10. evaporator thermal power ($\dot{Q}_{eva}$) versus working fluid mass flow rate ($\dot{m}_{wf}$), at different heat source temperatures ($T_{HW,in}$).

The performance of the evaporator is evaluated also by means of the total heat transfer effectiveness (ε_{eva}), which is calculated by virtually dividing the heat exchanger in two zones (economizer and vaporizer), and whose definition is reported in Equation (10).

$$\varepsilon_{eva} = \frac{\dot{Q}_{eco} + \dot{Q}_{vap}}{\dot{Q}_{eco\infty} + \dot{Q}_{vap\infty}} = \frac{\varepsilon_{eco} \cdot \dot{Q}_{eco\infty} + \varepsilon_{vap} \cdot \dot{Q}_{vap\infty}}{\dot{Q}_{eco\infty} + \dot{Q}_{vap\infty}} \tag{10}$$

where the symbols $\dot{Q}_{eco}$ and $\dot{Q}_{vap}$ refer to the thermal power exchanged in the economizer and vaporizer zone of the evaporator, respectively, the variables named ε_{eco} and ε_{vap} are the corresponding effectiveness, and the subscript ∞ identifies the ideal thermal power that would be transferred in case of infinite heat transfer surface. The value of ε_{eva} (Figure 11) increases with the reduction of the pinch point temperature difference, which is in general rather low in presence of partial evaporation (around 1-2 K), compared to the operation with dry expansion [10].

Figure 12 presents the values of the expander electrical power ($\dot{W}_{exp}$) and of the pump electrical consumption ($\dot{W}_{pump}$). At constant hot water temperature, the expander power decreases with the increment of the mass flow rate, due to the reduction of the vapour quality at the expander inlet, which causes lower amount of fluid vapour to expand inside the cylinders. The decreasing trend of $\dot{W}_{exp}$ at constant $T_{HW,in}$ is more visible with temperature equal to 60 °C and 75 °C, and in both cases the reduction is close to 200 W. As expected, a higher power output can be achieved with high heat source temperature. The peak of expander power is close to 1200 W, obtained with a heat source temperature of 75 °C and quality x_1 close to 1. The pump power consumption follows a different trend, increasing, at constant heat source temperature, with the increment of the mass flow rate. At constant $\dot{m}_{wf}$, the pump power consumption increases with the heat source temperature, due to the larger pressure difference that is achieved.

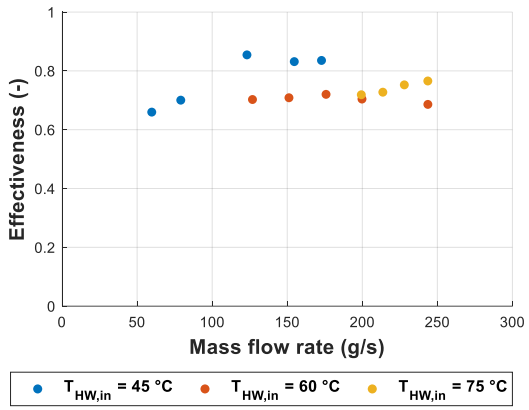

Figure 11. Evaporator effectiveness (ε_{eva}) versus working fluid mass flow rate ($\dot{m}_{wf}$), at different heat source temperatures ($T_{HW,in}$).

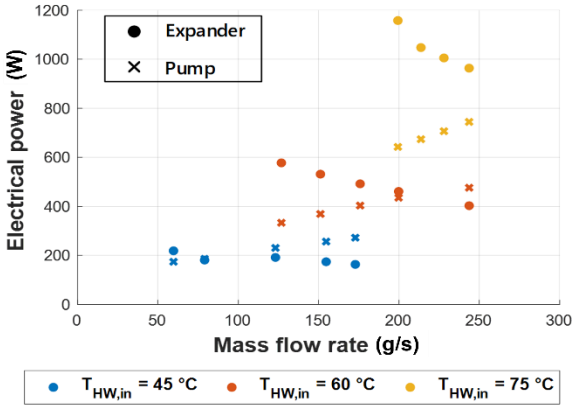

Figure 12. Expander and pump electrical power versus working fluid mass flow rate ($\dot{m}_{wf}$), at different heat source temperatures ($T_{HW,in}$).

The total efficiencies of the expander (η_{exp}) and of the pump (η_{pump}) are shown in Figure 13 versus the working fluid flow rate, for the different values of heat source temperature. The value of η_{exp}, at constant $T_{HW,in}$, decreases as the flow rate increases, and the trends are shifted to the right in the plot. A maximum expander efficiency around 36.5% is obtained with $T_{HW,in}$ of 45 °C and with vapour quality x_1 close to 1. The minimum value corresponds to a temperature of 75 °C and maximum mass flow rate close to 250 g/s, with vapour quality slightly higher than 0.7. On the contrary, the pump efficiency increases by increasing both $\dot{m}_{wf}$ and $T_{HW,in}$, with a peak around 37%, which is significantly higher than the maximum efficiency obtained in dry expansion conditions, close to 30%.

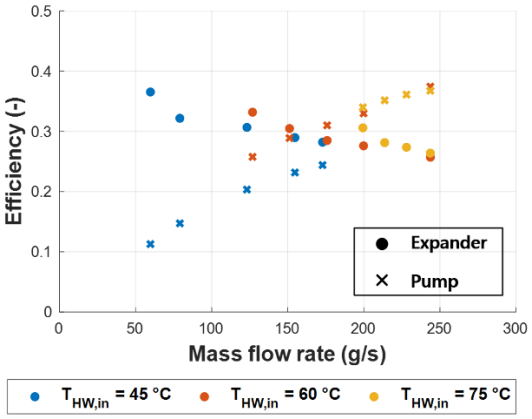

Figure 13. Total efficiency of expander (η_{exp}) and pump (η_{pump}) versus working fluid mass flow rate ($\dot{m}_{wf}$), at different heat source temperatures ($T_{HW,in}$).

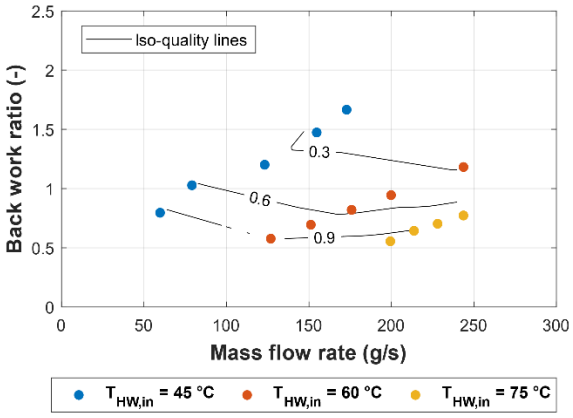

Figure 14. Back work ratio (BWR) versus mass flow rate ($\dot{m}_{wf}$), at different heat source temperatures ($T_{HW,in}$).

The very small size of the power plant, together with the relatively low performance of the machines and with the fact that the system is not optimized for working in partial evaporation mode, determines a remarkable impact of the feed pump consumption to the net power output, even though

the pump total efficiency has been improved by the PE operation. This aspect is evident at the lowest tested power output, which corresponds, according to Figure 12, also to the lowest values of the heat source temperature. This is confirmed by the trend of the back work ratio (BWR) in Figure 14, which shows that the pump absorbs more power than that produced by the expander, when the heat source temperature is equal to 45 °C, in all the conditions of working fluid flow rate (except one). The best condition (with BWR ≈ 50%) is obtained at quality close to 1 (hence with minimum flow rate), with temperature from 60 °C to 75 °C.

5. Conclusion

This paper presents an experimental analysis conducted on a partially evaporated micro-ORC, used for the conversion of ultra-low temperature (< 75 °C) heat into electricity. Even though the system on test bench is conceived for working with superheating conditions at the expander inlet (dry expansion), it demonstrated to be able to operate in condition of partial evaporation, thus with the expansion occurring entirely in the two-phase region. The thermodynamic properties of the working fluid inside the saturation curve are obtained using the open-source CoolProp library and the thermal balance on the heat exchangers, starting from the measured values of temperature, pressure and flow rate. The uncertainties of the key variables are assessed, including the uncertainty related to the calculation of the vapour quality of the organic fluid in the two-phase operating points.

The results highlight that the main difference, with respect to the dry expansion operation, is the increment of the mass flow rate of the working fluid, which produces the reduction of the vapour quality at the expander inlet; a negligible effect is visible on the evaporation pressure, which is mainly determined by the heat source temperature. The minimum vapour quality was close to 0.2.

Good performance of the evaporator can be obtained in partial evaporation mode, due to the reduction of the pinch point temperature difference, with respect to the operation with dry expansion. Maximum evaporator effectiveness close to 85% was achieved with the minimum tested heat source temperature of 45 °C. As expected, especially at high heat source temperature, the electrical power produced by the expander decreases with the increment of the working fluid mass flow rate (corresponding to the reduction of the vapour quality at the expander inlet). The maximum expander power output was close to 1200 W at temperature of 75 °C and vapour quality close to 1. The pump total efficiency increases with the mass flow rate and with the heat source temperature, achieving a maximum value around 37%. The analysis of the back work ratio (BWR) highlights that the performances of the expander and of the pump need to be optimized, in order to improve the net power output and make the system economically feasible.

References

[1] Tammone, C., Pili, R., Indrehus, S., Haglind, F., 2021. TECHNO-ECONOMIC ANALYSIS OF PARTIAL EVAPORATION ORGANIC RANKINE CYCLE SYSTEMS FOR GEOTHERMAL APPLICATIONS 10.

[2] Smith, I. K., 1993, Development of the trilateral flash cycle system Part 1 : fundamental considerations, Proceedings of the Institution of Mechanical Engineers, Part A: Journal of Power and Energy, vol. 207, no. 3, p. 179–194.

[3] Fischer, J., 2011. Comparison of trilateral cycles and organic Rankine cycles. Energy 36, 6208–6219. https://doi.org/10.1016/j.energy.2011.07.041

[4] Quoilin, S., Broek, M.V.D., Declaye, S., Dewallef, P., Lemort, V., 2013. Techno-economic survey of Organic Rankine Cycle (ORC) systems. Renewable and Sustainable Energy Reviews 22, 168–186. https://doi.org/10.1016/j.rser.2013.01.028.

[5] Cipollone, R., Bianchi, G., Di Bartolomeo, M., Di Battista, D., Fatigati, F., 2017. Low grade thermal recovery based on trilateral flash cycles using recent pure fluids and mixtures. Energy Procedia 123, 289–296. https://doi.org/10.1016/j.egypro.2017.07.246

[6] 'Brochure-HB-Products-HBX-CO2-v-2.pdf'. Accessed: Aug. 04, 2022. [Online]. Available: https://s3.eu-west-2.amazonaws.com/cdn.productsolutions.co.uk/2020/06/Brochure-HB-Products-HBX-CO2-v-2.pdf
[7] F. Dawo, J. Buhr, C. Wieland, and H. Spliethoff, 'EXPERIMENTAL INVESTIGATION OF THE PARTIAL EVAPORATED ORGANIC RANKINE CYCLE FOR VARIOUS HEAT SOURCE CONDITIONS', p. 9, 2021.
[8] M. A. Iqbal, S. Rana, M. Ahmadi, A. Date, and A. Akbarzadeh, 'Experimental study on the prospect of low-temperature heat to power generation using Trilateral Flash Cycle (TFC)', Applied Thermal Engineering, vol. 172, p. 115139, May 2020, doi: 10.1016/j.applthermaleng.2020.115139.
[9] D. Noël, P. Rivière, O. Cauret, D. Marchio, and C. Teuillières, 'Vapour quality determination for heat pumps using two-phase suction', International Journal of Refrigeration, vol. 131, pp. 766–774, Nov. 2021, doi: 10.1016/j.ijrefrig.2021.08.020.
[10] S. Ottaviano, C. Poletto, M. A. Ancona, and F. Melino, "Experimental investigation on micro-ORC system operating with partial evaporation and two–phase expansion," Energy Convers. Manag., vol. 274, p. 116415, Dec. 2022, doi: 10.1016/j.enconman.2022.116415.
[11] Bianchi, M., Branchini, L., Casari, N., De Pascale, A., Melino, F., Ottaviano, S., Pinelli, M., Spina, P.R., Suman, A., 2019. Experimental analysis of a micro-ORC driven by piston expander for low-grade heat recovery. Applied Thermal Engineering 148, 1278–1291. https://doi.org/10.1016/j.applthermaleng.2018.12.019.
[12] I.H. Bell, J. Wronski, S. Quoilin, V. Lemort, Pure and pseudo-pure fluid thermophysical property evaluation and the open-source thermophysical property library CoolProp, Ind. Eng. Chem. Res 53 (6) (2014) 498–508, https://doi.org/10.1021/ie4033999.
[13] Zampieri G. "CLOSED-CYCLE PLANT." U.S. Patent No. 20,160,032,786. 4 Feb. 2016.
[14] Bianchi, M., Branchini, L., Casari, N., Pascale, A.D., Fadiga, E., Melino, F., Ottaviano, S., Peretto, A., Pinelli, M., Spina, P.R., Suman, A., 2019. Uncertainty quantification of performance parameters in a small scale ORC test rig. Proceedings of the 5th International Seminar on ORC Power Systems 9 - 11 September 2019, Athens, Greece.